ADVANCED OPTICAL MATERIALS

www.advopticalmat.de

Self-Filtered Narrowband Perovskite Photodetectors with Ultrafast and Tuned Spectral Response

Lingliang Li, Yehao Deng, Chunxiong Bao, Yanjun Fang, Haotong Wei, Shi Tang, Fujun Zhang, and Jinsong Huang**

Combining bandpass filters with broadband photodetectors is the most common way to detect light within a specific spectral range in many applications that need to detect only the light within desired spectral range. Here, a method is reported to realize narrowband spectral response of perovskite photodetectors by applying hybrid perovskites layers with the same or a slightly larger bandgap as filters, which are integrated into perovskite photodetectors. The narrowband photodetectors have a full width at half maximum of 28 nm due to the sharp absorption edges of perovskite materials, and the light rejection ratio is above 1000. By tuning the bandgaps of perovskite filters and the associated perovskite layers in the detectors, the response bands are continuously tuned in the whole visible light region to satisfy different applications. Superior to the thick single crystal narrowband perovskite photodetectors, the naorrowband peroskite detectors with this design have a very high response speed only limited by the resistance capacitance constant.

Narrowband photodetection is broadly applied in many applications where light within only a specific wavelength needs to be detected, while light within other wavelength range needs to be rejected or cause no response to a photodetector. For example, flames detection requires solar-blind ultraviolet photodetectors to avoid false signal caused by other light source such as the sunlight[1]; Digital imagers or cameras need color-selective light sensors to record the red (R), green (G), or blue (B) light, respectively[2]; Fluorescent labeling of biomolecules requires photodetectors to be sensitive to photoluminescence of the analytes, but blind to excitation light.[3] The common practice in these applications is to combine bandpass optical filters with a broadband photodetectors is to achieve narrowband detection.

A new method was proposed by *Meredith* to achieve narrowband photodetectors by taking advantage of the difference between the light absorption and charge extraction distance, using thick organic active layer in a metal/organic/metal sandwich structure.[4] These detectors have a narrowband response to light close to the band-edge, however external quantum efficiency of these device is below 30% the device, because only collect a small portion of photogenerated charges in these narrowband photodetectors.[5] A similar method was also proposed to achieve narrowband photoconductors with gain, based on organic semiconductor mixed with inorganic quantum dots as charge traps.[6] Later on, narrowband photoconductors using all-organic active layer with gain was also realized by replacing nanoparticles with a small amount of fullerene derivative [6,6]-phenyl-C71-butyric acid methyl ester (PCBM) with percentage of PCBM below the percolation limit.[7] However the response speed of such detectors are generally slow, limited by the very small mobility of organic semiconductors, thick active layers as well as the long charge-trapping lifetime.

Recently, organic–inorganic halide perovskite photodetectors with superior performance to silicon photodetectors are reported.[8] Key parameters, including response speed,[8a,b] specific detectivity,[8c,d] and external quantum efficiency (EQE)[8e,f] of perovskite photodetectors are already comparable or even better than those of commercial silicon photodetectors. One of the major merit of perovskite photodetectors is the short response time of sub-nanosecond,[8b] due to short transit time enabled by high mobility and strong light absorption of perovskites.[9] Perovskite photodiodes have high internal efficiency even in self-powered operation mode (zero bias) due to long charge diffusion length in these materials.[10,11] However, the long charge diffusion length makes it difficult to realize narrowband perovskite photodetectors using the thick-active-layer method mentioned above. Theoretically, simply increasing active layer thickness, even up to millimeter, is not enough to produce narrowband perovskite photodetectors with high rejection ratio (see simulation results in the Supporting Information). Nevertheless, it is noted that narrowband perovskite photodetectors were indeed realized using perovskite single crystals with thickness down to micrometers, and such narrowband photodetectors had rejection ratio of above 200

L. Li, Y. Deng, Dr. C. Bao, Dr. Y. Fang, Dr. H. Wei, S. Tang, Prof. J. Huang
Department of Mechanical and Materials Engineering and Nebraska Center for Materials and Nanoscience
University of Nebraska-Lincoln
Lincoln, NE 68588, USA
E-mail: jhuang@unc.edu, jhuang2@unl.edu

L. Li, Prof. F. Zhang
Key Laboratory of Luminescence and Optical Information
Ministry of Education
Beijing Jiaotong University
Beijing 100044, P. R. China
E-mail: fjzhang@bjtu.edu.cn

Prof. J. Huang
Department of Applied Physical Sciences
University of North Carolina
Chapel Hill, NC 27599, USA

DOI: 10.1002/adom.201700672

with a FWHM of smaller than 20 nm.[12] The narrowband response in these detectors originates from the strong surface-charge recombination which quenches photogenerated charges by short-wavelength light. However, the thick crystals used increased the response time to several milliseconds despite of the relatively high mobility of perovskite single-crystals, much longer than the sub-nanosecond response time of thin film perovskite photodetectors.

In this work, we demonstrate a new method to tune the spectral response band of perovskite photodetectors with perovskite filters. Narrowband perovskite photodetectors based on this method have good color selectivity with FWHM of 28 nm and rejection ratio of >1000, while maintain the major advantages of perovskite thin film photodetectors such as quick response speed. Red-Green-Blue (RGB) perovskite photodetectors are realized to demonstrate that response band can be easily controlled with this method.

The central idea to realize the narrowband photodetector is to introduce an optically-active-but-electronically-dead layer in the detector, which only absorbs short-wavelength light while, does not generate photocurrent. As illustrated in **Figure 1**a, an optically-active-but-electronically-dead area close to the transparent electrode is in the active layer of previously reported narrowband photodetector based on thick active layer. Charges generated by short-wavelength light in this area are supposed to recombine nonradiatively before they transport to the other electrode because the diffusion length of carrier in these materials is shorter than the total thickness of the thick films. It is noted this very thick layer did affect the device response speed. In our new design, we separate this optically-active-but-electronically-dead area from the device by removing it from the photoactive layer, and putting it onto the glass to become an independent layer. The device structure is perovskite-1/transparent-conductive window/perovskite-2/electrode, as illustrated in Figure 1b. Here, perovskite-1 and perovskite-2 layers can be the same or different, but the bandgap of perovskite-1 is not smaller than that of perovskite-2. Perovskite-1 layer only absorbs light, and photogenerated charges in it will not contribute to photocurrent, because it is electrically isolated from the electrodes. In this case, perovskite-2 layer does not need to be very thick to exceed charge diffusion length. The absorption edges of perovskite-1 and perovskite-2 layers will determine the responding band of the photodetectors. Since only a small portion of light can be absorbed by perovskite-2, such devices have narrowband response. Their response speed is determined by the photodetectors with perovskite-2 as the active layer which can be very fast. In this study, perovskite-1 and perovskite-2 layers can be mixed-halide perovskite, so that absorption edge is tunable all the way from ≈400 nm for $MAPbCl_3$ to ≈800 nm for $MAPbI_3$ to cover the whole visible spectral range.

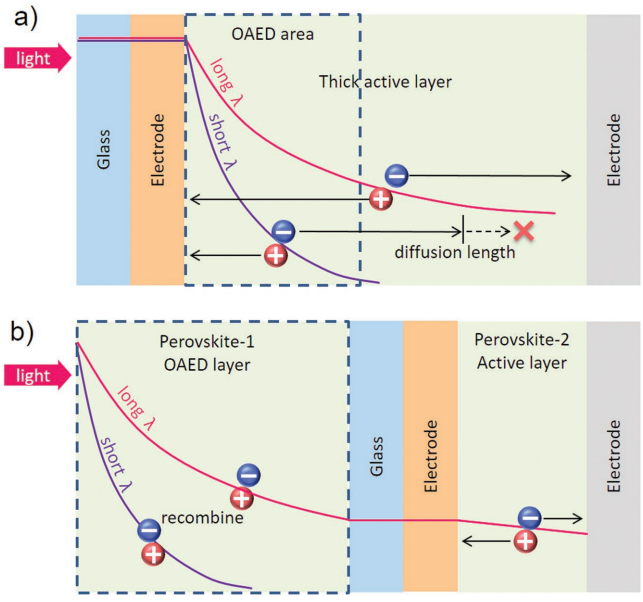

Figure 1. a) Schematic showing narrowband photodetector with thick active layer. Near surface area of active layer is optically-active-but-electronically-dead (OAED). Charges generated by short wavelength light in this area are harder to be collected due to limited diffusion length. Long wavelength incident light can generate charges deep in bulk, which are easier to be collected, and contribute to a narrow response band. b) Schematic showing narrowband photodetector with our new design. A normal photodiode is integrated with optically-active-but-electronically-dead semiconductor layer. Charges generated in this layer will only stay in this layer and cannot be collected. Long wavelength incident light can penetrate through this layer into the active layer, and contribute to a narrow response band.

To demonstrate this idea, we first fabricated photodetectors with narrowband response spectrum locating at ≈780 nm. The device structure was perovskite-1/glass/indium tin oxide (ITO)/poly(bis(4-phenyl)(2,4,6-trimethylphenyl)amine) (PTAA)/perovskite-2/[6,6]-phenyl-C61-butyricacid methyl ester (PCBM)/C60/2,9-dimethyl-4,7-diphenyl-1,10-phenanthroline (BCP)/copper (Cu), as shown in **Figure 2**a. The perovskite-1 layer was $MAPbBr_{3-x}I_x$ with Br:I ratio of 1:3, 1:8, and 1:16, respectively. Perovskite-2 layer was $MAPbI_3$. The perovsktie detectors with structure of glass/ITO/PTAA/perovskite-2/PCBM/C_{60}/BCP/Cu were optimized based on our previous studies.[13] The thickness of perovskite-1 layer was 12 µm. For comparison, we also fabricated a device with a structure shown in Figure 2b where the thickness of the $MAPbI_3$ active layer is 20 µm.

EQE spectra of these devices were measured with a Newport incident photon-to-electron conversion efficiency (IPCE) measurement system under zero bias and 8 Hz modulated light, and the results are shown in Figure 2c. The device with 20 µm thick active layer still shows a broad spectral response, because photogenerated charges close to the light incident window can be transported to cathode, and the shorter wavelength EQE is not suppressed. Thick active layer device has an EQE cutting edge at ≈825 nm, which is different from that at ≈800 nm for standard perovskite solar cells. This is because the thick perovskite layers can harvest more photons at Urbach tail than the thin perovskite layers, when absorption coefficient at Urbach tail is relatively small. In contrast, devices with integrated perovskite-1 layer show narrowband response. Perovskite-1 layer of $MAPbBr_{3-x}I_x$ has a slightly blueshifted absorption edge comparing with perovskite-2 layer of neat $MAPbI_3$. A gap between the absorption edges of perovskite-1 and perovskite-2 layers is created. The gap allows more photons to penetrate through perovskite-1 layer and then be absorbed by perovskite-2 layer. To demonstrate the advantages of using mixed-halides perovskite as the perovskite-1 layer, a device with neat $MAPbI_3$ for both

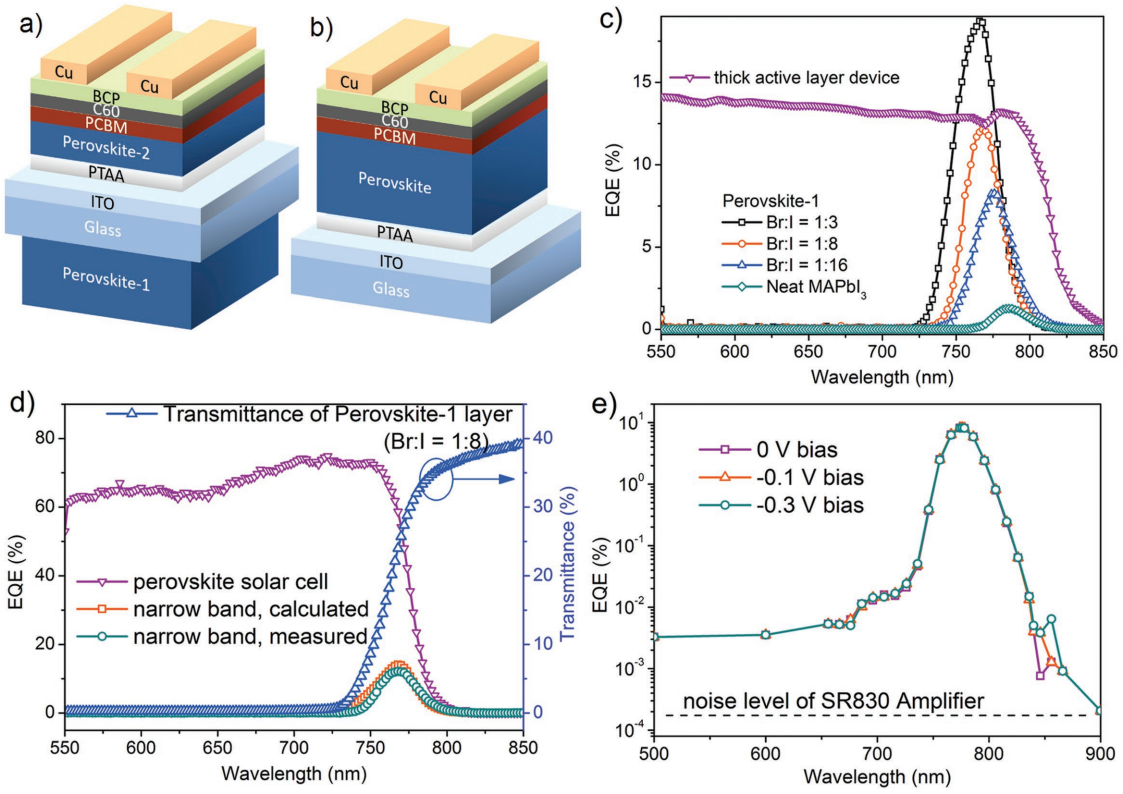

Figure 2. a) Device structure of a perovskite photodiode combining a thick perovskite layer as an optical filter in front of light incident window. b) Device structure of perovskite photodiode with thick active layer. c) EQE spectra of device with thick active layer and devices with integrated perovskite-1 filter layer with different mixed-halides ratios. d) Calculated narrowband device's EQE as the product of filter's transmittance and solar cell's EQE. Calculated result well matches measured result. e) Accurate EQE spectra recorded using a SR830 lock-in amplifier in low noise environment, plotted as semilogarithmic.

perovskite-1 and perovskite-2 layers was fabricated and its EQE spectrum is shown in Figure 2c. The short wavelength EQE of this device is not well suppressed and the peak EQE of this device is smaller, compared with the devices with mixed-halides perovskite-1 layers. It turns out that using the same material as both filter and active layer is not an efficient way to achieve narrowband photodetector with high EQE. All the devices with integrated perovskite-1 layers show narrowband with FWHM of ≈30 nm, which is comparable to that (<20 nm) of our previously reported narrowband photodetectors based on single crystals. The narrowband photodetectors based on thick single crystals have narrower response band because of better crystallinity and purity, and thus sharper absorption edge than polycrystalline films have. Among the narrowband devices studied here, the device with Br:I ratio of 1:8 in perovskite-1 layer has the smallest FWHM of 28 nm, so it is chosen for the following measurements. The reason it has smallest FWHM is that it utilizes the two absorption edges at the position with the biggest slopes in the plots of absorption coefficient versus wavelength. We calculated the EQE shape of the narrowband devices based on the product of the transmittance of the perovskite-1 layer and the EQE of the underneath perovskite photodetector. As shown in Figure 2d, calculated EQE spectrum is very close to the measured EQE spectrum of the device.

The device rejection ratio, defined as the ratio of peak EQE and the smallest EQE measured at short wavelength range, is a most important parameter for narrowband photodetectors. The EQE of the narrowband photodetectors at short wavelength range has been suppressed to be lower than the noise of IPCE system. To accurately measure the rejection ratio, the narrowband photodetectors were transferred into a low noise environment, and its EQE was carefully measured with a high sensitivity SR830 lock-in amplifier. The measured EQE is shown in Figure 2e with a semilogarithmic plot. The rejection ratio measured is larger than 1000. Shorter wavelength EQE was insensitive to increased reverse bias (Figure 2e), which is different from the narrowband perovskite photodetectors based on single crystals and make these devices more attractive for applications for a faster respond speed.[12] It also indicates that internal quantum efficiency has already saturated at zero bias condition, which should be attributed to good transport properties and low charge recombination rate in high quality perovskite-2 layer.

Good transport properties and low recombination rate imply that weak light detection ability of these devices may also be good. We used SR830 lock-in amplifier to measure photocurrent as a function of incident light intensity, and the result is shown in **Figure 3**a. The device showed linear response to incident light with intensity from 13.6 pW cm^{-2} to 46.7 mW cm^{-2}, corresponding to a linear dynamic range (LDR) of 190 dB. The weakest light intensity the device can distinguish from noise is 13.6 pW cm^{-2}, which is also defined as noise equivalent

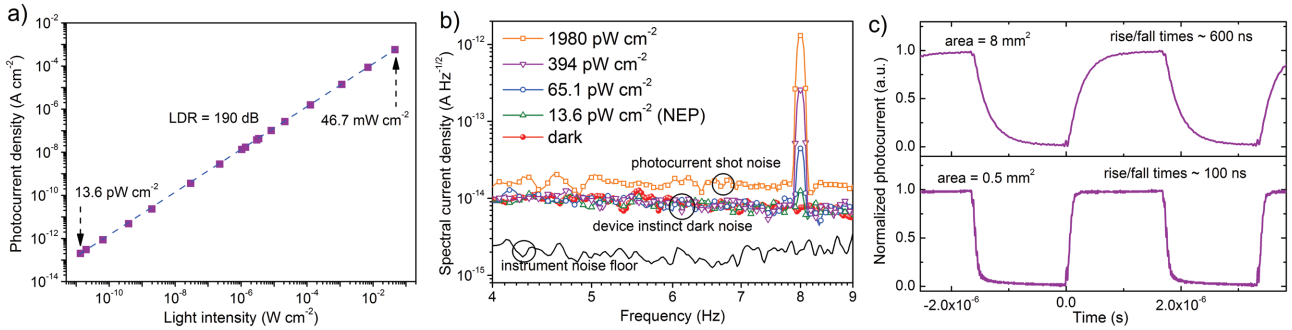

Figure 3. a) LDR of the narrowband perovskite photodetector, the lowest measurable light intensity is 13.6 pW cm^{-2}. b) Spectral current density of device in dark, and under different intensities' illuminations. c) TPC of devices with 8 and 0.5 mm^2 area.

power (NEP). To confirm the NEP and further calculate specific detectivity (D^*), we measured the device's noise with a fast Fourier transformation (FFT) analyzer combined with a low-noise current preamplifier. The measured noise spectral current density is shown in Figure 3b. The noise of the device is $\approx 8 \times 10^{-5}$ A Hz^{-1} at 8 Hz. This setup also allows the measurement of NEP directly by reducing light intensity and record the signal in the same way of recording noise. As shown in Figure 3b, the signal at 8 Hz merged into noise when the light intensity reduced to 13.6 pW cm^{-2}. Specific detectivity (D^*) is NEP normalized by square root of device area (A) and bandwidth (B), and can be directly calculated with spectral noise density (S_{noise}) as

$$D^* = \frac{\sqrt{AB}}{NEP} = \frac{R\sqrt{A}}{S_{noise}} \quad (1)$$

where R is responsivity. The peak EQE of the device is about 12.1% (Figure 2c), corresponding to a responsivity of 0.076 A W^{-1}. Calculated specific detectivity of our device at 8 Hz is 2.65×10^{-12} cm $\sqrt{\text{Hz}}$W^{-1}. It is slightly smaller than that of our reported low-noise broadband perovskite photodetector.[14] due to the loss of absorption with the perovskite-1 filter layer. However, this D^* value is still at least one order of magnitude higher than those of previously reported narrowband perovskite photodetectors,[12,15] and is comparable to commercial silicon photodetectors (e.g., 2.2×10^{-12} cm $\sqrt{\text{Hz}}$W^{-1} for Newport model 818-UV photodetector).

One important advantage of this device design is that the device respond speed is in principle only limited by resistance capacitance (RC) constant of the measurement circuit. Transient photocurrent (TPC) of devices under illumination of a 780 nm light emitting diode (LED) modulated at 300 kHz was recorded by an oscilloscope, and the TPC results are shown in Figure 3c. The rise/fall time of the LED used in this experiment is 80 ns. The 8 and 0.5 mm^2 devices have response times of ≈600 ns and ≈100 ns, respectively. The 0.5 mm^2 device has the faster response speed due to its smaller RC constant. It is reasonable to believe that if the narrowband perovskite photodetector was further optimized by removing low mobility PCBM layer[17] and reducing the active area, the response time could be decreased to sub-nanosecond, as we reported earlier.[8b]

Finally, we demonstrated that the spectral response could be tuned by changing the mixed halides ratios in perovskite-1 and perovskite-2 layers. To manifest the easy tuning of spectral response, we made the spectral response of three types of perovskite narrowband photodetectors to match the sensitivity of human cone cells with attempting to mimic human eye's color sensitivity. For the blue light photodetector, perovskite-1 layer is neat $MAPbCl_3$ and perovskite-2 layer is $MAPbCl_{1.5}Br_{1.5}$. For the green light photodetector, perovskite-1 layer is $MAPbCl_{1.2}Br_{1.8}$ and perovskite-2 layer is $MAPbBr_{1.5}I_{1.5}$. For the red light photodetector, perovskite-1 layer is neat $MAPbBr_3$ and perovskite-2 layer is $MAPbBr_2I$. The upper panel of **Figure 4** shows EQE spectra of three perovskite photodetectors, which were designed to match the sensitivity of human eye to red, green, and blue colors shown in the lower panel of Figure 4. The EQE spectrum of blue light photodetector shows half maximum EQE value at about 421 and 487 nm locations, which are closed to 418 and 475 nm for human eye's blue cone cell, respectively. Similar results can be observed when comparing those of green light photodetector (506 and 616 nm) to human eye's green cone cell (509 and 614 nm), and red light photodetector (567 and 648 nm) to human eye's red cone cell (558 and 635 nm). Nowadays, silicon-based photodetectors need multiple filters[16] to adjust their spectral response to match color detection.[17] Commercial image sensors are usually based on silicon photodetectors combined with RGB color filters and an

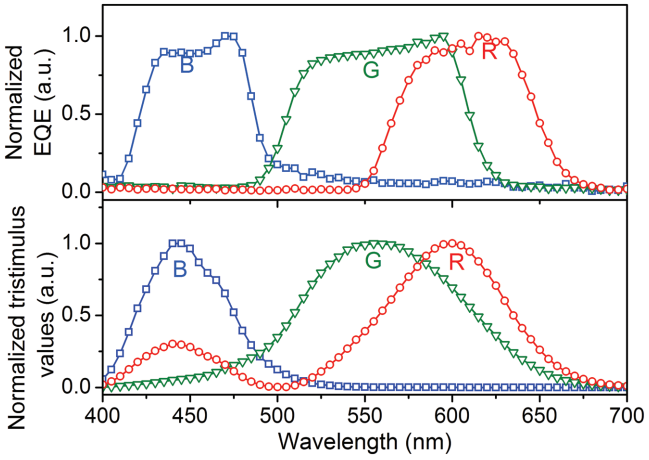

Figure 4. Standard color matching functions (CIE S 014-1/E:2006) of human eye's cone cells, and EQE spectra of three perovskite photodetectors designed to match the functions.

additional infrared-blocking filter. The infrared-blocking filter is needed, because silicon photodetectors are sensitive to infrared light due to smaller bandgap than perovskites.[16b] Due to the adjustable bandgap, the perovskite RGB photodetectors only have one layer of filter (perovskite-1 layer), which is an advantage for low-cost image sensing applications.

In summary, we reported a design to achieve perovskite narrowband photodetectors with tunable spectral response in the whole visible light range. The response band can be adjusted to be as narrow as 28 nm in FWHM, and can be wider. Rejection ratio higher than 1000 was demonstrated. The narrowband perovskite photodetectors have the advantages of regular perovskite photodetectors, such as high specific detectivity of 2.65×10^{-12} cm $\sqrt{\text{Hz}}\text{W}^{-1}$, large LDR of 190 dB, and fast response speed of >10 MHz. We further demonstrated that the RGB perovskite photodetectors have spectral response matching that of human eyes. The combination of printing technology will enable the image sensor fabrication at high throughput and low cost in the future.

Experimental Section

Perovskite Material Preparing: Methylammonium iodide (MAI) and Lead(II) iodide (PbI_2) were dissolved into *N*,*N*-dimethylformamide (DMF) to prepare $MAPbI_3$ solution. Methylammonium bromide (MABr) and Lead(II) iodide ($PbBr_2$) were dissolved into DMF to prepare $MAPbBr_3$ solution. Methylammonium chloride (MACl) and Lead(II) chloride ($PbCl_2$) were dissolved into DMF to prepare $MAPbCl_3$ solution. All three solutions had concentration of 1 mol L^{-1}. The mixed-halide perovskite solutions were prepared by mixing these solutions with different ratios. Before spin coating $MAPbI_3$ film, 10% of dimethyl sulfoxide (DMSO) was added into $MAPbI_3$ solution.[13a] In doctor-blade coating process, DMSO was not added.

Device Fabrication: All perovskite-1 filters were prepared by doctor-blade coating[18] mixed-halide perovskite solutions onto clean glass substrates, and then thermal annealed at 100 °C in air for 1 h. The fabrication process of standard perovskite solar cell with $MAPbI_3$ as active layer is as same as literature.[13a] PTAA layer was deposited on ITO/glass by spin coating 0.2 wt% PTAA in toluene at 4000 rpm for 35 s onto ITO/glass substrate. Then the PTAA coated substrate was thermally annealed at 100 °C for 10 min. The $MAPbI_3$ precursor solution was spin coated at 2000 rpm for 2 s and 4000 rpm for 20 s onto PTAA layer. After the $MAPbI_3$ precursor solution was coated, toluene was drop-casted onto the sample to quickly precipitate $MAPbI_3$. Then the sample was annealed at 65 °C for 10 min and 100 °C for 10 min. PCBM layer was coated by spinning 2 wt% PCBM in dichlorobenzene at 6000 rpm for 35 s and then annealed at 100 °C for 30 min. After that, 20 nm C_{60}, 8 nm BCP, and 80 nm Cu was sequentially deposited by thermal evaporation. Finally, the perovskite-1 filter and standard perovskite solar cell were glued together to complete the device. Devices with mixed-halide perovskite as active layer were fabricated by similar process, the only difference is that the active layer is doctor-blade coated.[18]

Photodetector Characterization: EQE spectra in Figures 2c and 1d were measured with a Newport IPCE measurement system under zero bias and 8 Hz modulated light. Accurate EQE spectra in Figure 2e were measured by SR830 lock-in amplifier connected to the device under 8 Hz modulated light with different wavelengths. Bias on the device was applied by a battery. The linear dynamic range was measured by a SR830 lock-in amplifier connected to the devices under illumination with different light intensities and modulated at 8 Hz. Light intensity was calibrated by a Si photodetector (Hamamatsu model S2387-33R). Light source is a 780 nm LED (Thorlabs model LED780E) powered by a function generator. Noise signal of the device was first preamplified with a SR570 low-noise current amplifier and then recorded and analyzed with an Agilent35670A FFT analyzer. TPC was measured with a digital oscilloscope (Agilent DSO-X 3104A), while the 780 nm LED was modulated at 300 kHz by the function generator. The perovskite-1 filter transmittance spectrum was measured with a LAMBDA 1050 UV/Vis/NIR Spectrophotometer.

Supporting Information

Supporting Information is available from the Wiley Online Library or from the author.

Acknowledgements

This work was financially supported by National Science Foundation under Award No. ECCS-1608610. F.Z. thanks the financial support from National Natural Science Foundation of China (Nos. 61377029 and 61675017). L.L. thanks Fundamental Research Funds for the Central Universities (No. 2015YJS176), Beijing Jiaotong University (No. 13118423), and China Scholarship Council (No. 201607090039), that supported his visit at University of Nebraska Lincoln.

Conflict of Interest

The authors declare no conflict of interest.

Keywords

perovskites, photodetectors, narrowband

Received: July 8, 2017
Revised: July 30, 2017
Published online: September 14, 2017

[1] a) M. Razeghi, A. Rogalski, *J. Appl. Phys.* **1996**, *79*, 7433; b) D. Walker, V. Kumar, K. Mi, P. Sandvik, P. Kung, X. H. Zhang, M. Razeghi, *Appl. Phys. Lett.* **2000**, *76*, 403.

[2] a) S. Kawada, S. Sakai, N. Akahane, R. Kuroda, S. Sugawa, presented at *2009 IEEE Sensors Conf.* Christchurch, New Zealand, October 2009; b) W. Kim, W. Yibing, I. Ovsiannikov, S. Lee, Y. Park, C. Chung, E. Fossum, presented at *2012 IEEE Int. Solid-State Circuits Conf.* San Francisco, CA, February 2012.

[3] U. Resch-Genger, M. Grabolle, S. Cavaliere-Jaricot, R. Nitschke, T. Nann, *Nat. Methods* **2008**, *5*, 763.

[4] A. Armin, R. D. Jansen-van Vuuren, N. Kopidakis, P. L. Burn, P. Meredith, *Nat. Commun.* **2015**, *6*, 6343.

[5] V. Coropceanu, J. Cornil, D. A. da Silva Filho, Y. Olivier, R. Silbey, J.-L. Brédas, *Chem. Rev.* **2007**, *107*, 926.

[6] a) L. Shen, Y. Zhang, Y. Bai, X. P. Zheng, Q. Wang, J. S. Huang, *Nanoscale* **2016**, *8*, 12990; b) L. Shen, Y. Fang, H. Wei, Y. Yuan, J. Huang, *Adv. Mater.* **2016**, *28*, 2043.

[7] W. Wang, F. Zhang, M. Du, L. Li, M. Zhang, K. Wang, Y. Wang, B. Hu, Y. Fang, J. Huang, *Nano Lett.* **2017**, *17*, 1995.

[8] a) L. Shen, Y. Z. Lin, C. X. Bao, Y. Bai, Y. H. Deng, M. M. Wang, T. Li, Y. F. Lu, A. Gruverman, W. W. Li, J. S. Huang, *Mater. Horiz.* **2017**, *4*, 242; b) L. Shen, Y. Fang, D. Wang, Y. Bai, Y. Deng, M. Wang, Y. Lu, J. Huang, *Adv. Mater.* **2016**, *28*, 10794; c) Q. Q. Lin, A. Armin, D. M. Lyons, P. L. Burn, P. Meredith, *Adv. Mater.* **2015**, *27*, 2060; d) L. Gao, K. Zeng, J. Guo, C. Ge, J. Du, Y. Zhao, C. Chen, H. Deng,

Y. He, H. Song, G. Niu, J. Tang, *Nano Lett.* **2016**, *16*, 7446; e) R. Dong, Y. J. Fang, J. Chae, J. Dai, Z. G. Xiao, Q. F. Dong, Y. B. Yuan, A. Centrone, X. C. Zeng, J. S. Huang, *Adv. Mater.* **2015**, *27*, 1912; f) Y. Lee, J. Kwon, E. Hwang, C. H. Ra, W. J. Yoo, J. H. Ahn, J. H. Park, J. H. Cho, *Adv. Mater.* **2015**, *27*, 41; g) Z. Lian, Q. Yan, Q. Lv, Y. Wang, L. Liu, L. Zhang, S. Pan, Q. Li, L. Wang, J.-L. Sun, *Sci. Rep.* **2015**, *5*, 16563; h) X. Hu, X. Zhang, L. Liang, J. Bao, S. Li, W. Yang, Y. Xie, *Adv. Funct. Mater.* **2014**, *24*, 7373.

[9] a) H. Zhou, Q. Chen, G. Li, S. Luo, T.-B. Song, H.-S. Duan, Z. Hong, J. You, Y. Liu, Y. Yang, *Science* **2014**, *345*, 542; b) W. S. Yang, J. H. Noh, N. J. Jeon, Y. C. Kim, S. Ryu, J. Seo, S. I. Seok, *Science* **2015**, *348*, 1234; c) D. Bi, W. Tress, M. I. Dar, P. Gao, J. Luo, C. Renevier, K. Schenk, A. Abate, F. Giordano, J.-P. Correa Baena, J.-D. Decoppet, S. M. Zakeeruddin, M. K. Nazeeruddin, M. Grätzel, A. Hagfeldt, *Sci. Adv.* **2016**, *2*, e1501170.

[10] Q. Dong, Y. Fang, Y. Shao, P. Mulligan, J. Qiu, L. Cao, J. Huang, *Science* **2015**, *347*, 967.

[11] H. Zhou, Z. H. Song, P. Tao, H. W. Lei, P. B. Gui, J. Mei, H. Wang, G. J. Fang, *RSC Adv.* **2016**, *6*, 6205.

[12] Y. J. Fang, Q. F. Dong, Y. C. Shao, Y. B. Yuan, J. S. Huang, *Nat. Photonics* **2015**, *9*, 679.

[13] a) B. Chen, Y. Bai, Z. Yu, T. Li, X. Zheng, Q. Dong, L. Shen, M. Boccard, A. Gruverman, Z. Holman, J. Huang, *Adv. Energy Mater.* **2016**, *6*, 1601128; b) Y. Lin, L. Shen, J. Dai, Y. Deng, Y. Wu, Y. Bai, X. Zheng, J. Wang, Y. Fang, H. Wei, W. Ma, X. C. Zeng, X. Zhan, J. Huang, *Adv. Mater.* **2016**, *29*, 1604545.

[14] Y. J. Fang, J. S. Huang, *Adv. Mater.* **2015**, *27*, 2804.

[15] Q. Q. Lin, A. Armin, P. L. Burn, P. Meredith, *Nat. Photonics* **2015**, *9*, 687.

[16] a) R. Lukac, K. N. Plataniotis, *IEEE Trans. Consum. Electron.* **2005**, *51*, 1260; b) L. Frey, P. Parrein, J. Raby, C. Pellé, D. Hérault, M. Marty, J. Michailos, *Opt. Express* **2011**, *19*, 13073.

[17] G. Wyszecki, W. S. Stiles, *Color Science*, Wiley, New York **1982**.

[18] Y. Deng, Q. Wang, Y. Yuan, J. Huang, *Mater. Horiz.* **2015**, *2*, 578.